Langmuir

Article

Toughness Governs the Rupture of Interfacial H-bond Assemblies at a Critical Length Scale in Hybrid Materials

Navid Sakhavand, Prakash Muthuramalingam, and Rouzbeh Shahsavari

Just Accepted

1
2
3
4
5
6
7
8
9
10
11
12
13
14
15
16
17
18
19
20
21
22
23
24
25
26
27
28
29
30
31
32
33
34
35
36
37
38
39
40
41
42
43
44
45
46
47
48
49
50
51
52
53
54
55
56
57
58
59
60

Toughness Governs the Rupture of Interfacial H-bond Assemblies at a Critical Length Scale in Hybrid Materials

By

Navid Sakhavand,[1] Prakash Muthuramalingam[1] and Rouzbeh Shahsavari[1,*]

[1]Department of Civil and Environmental Engineering, Rice University, Houston, TX 77005

*Corresponding-Author (Email: rouzbeh@rice.edu)

Keywords: Hydrogen bonds, toughness, Interface mismatch, Load transfer, Polymer-silicates interactions.

Abstract. The geometry and material property mismatch across the interface of hybrid materials with dissimilar building blocks make it extremely difficult to fully understand the lateral chemical bonding processes and design nanocomposites with optimal performance. Here, we report a combined first-principles study, molecular dynamics modeling and theoretical derivations to unravel the detailed mechanisms of H-bonding, deformation, load transfer and failure at the interface of Polyvinyl alcohol (PVA) and silicates, as an example of hybrid materials with geometry and property mismatch across the interface. We identify contributing H-bonds that are key to adhesion and demonstrate a specific periodic pattern of interfacial H-bond network dictated by the interface mismatch and intra-molecular H-bonding. We find that the maximum toughness, incorporating both intra- and inter-layer strain energy contributions, govern the existence of optimum overlap length and thus the rupture of interfacial (inter-layer) H-bond assemblies in natural and synthetic hybrid materials. This universally valid result is in contrast to the previous reports that correlate shear strength with rupture of H-bonds assemblies at a finite

1

overlap length. Overall, this work establishes a unified understanding to explain the interplay between geometric constraints, interfacial H-bonding, materials characteristics and optimal mechanical properties in hybrid organic-inorganic materials.

1. INTRODUCTION

By combining platelet-like ceramic building blocks and organic matrices nature creates hybrid materials such as bone, teeth and mollusk shells that have outstanding balance of stiffness, strength and flaw-tolerance.[1-3] This has inspired fabrication of several advanced human-made polymer-matrix composites with inorganic reinforcing materials such as cement, clays, glass, graphite, SiC, and mica.[4-7] In these hybrid materials, the adhesion and load transfer between organic and inorganic constituents at the nano-scale is a complex process that mainly trace back to the cooperative action of several chemical bonds. Considering hydrogen-bond (H-bond) network as the source of interfacial interactions, previous studies have primarily focused on either the average response of such hybrid materials under shear load, *e.g.* graphene oxide composite paper [8,9] or the detailed processes of shear load transfer only between identical building blocks such as -sheets in spider silk[10-12], where the H-bond donor (guest) and the H-bond acceptor (host) sites for H-bonding are aligned in parallel. Despite the importance of the lateral H-bonding, there is currently no fundamental understanding (to our knowledge) on detailed mechanisms of interfacial interactions in hybrid materials where there is a mismatch between the guest and host sites across the interface.

To address this issue and illustrate our purpose, here we focus on synthetic polymer-silicates as a subclass of hybrid organic-inorganic materials and map out the inherent, non-

2

intuitive characteristics of interfacial H-bonding and load transfer in these hybrid materials. A prime example of synthetic polymer-silicates is introduction of polymers in Calcium-Silicate-Hydrate (C-S-H) gel,[13-16] where the latter is the main product of cement hydration.[17] With Zeolitic-type pores and inter-laminar distances of a few angstroms, C-S-H provides an excellent system to host polymers in confined spaces and study their hybrid chemical and physical behavior. Recent syntheses of various polymer C-S-H systems have shown enhanced material properties.[18-22] X-ray diffraction (XRD), Nuclear Magnetic Resonance (NMR) and Fourier Transform Infrared spectroscopy (FTIR) experiments on polymer modified C-S-H reveal the intercalation of the polymer chains into the nanopores of the C-S-H.[19,23,24] There are reports on synthesized polymer modified C-S-H with several water-soluble polymers and incorporation of organic groups in C-S-H without disrupting its inorganic framework.[15,23] These experimental works suggested proximity of ethyl groups to the silica tetrahedra in C-S-H. Later, Mojumdar *et al.*[24] reported H-bonding between C-S-H and Polyvinyl Alcohol (PVA) by monitoring the shift in frequencies of FTIR spectra. In another study, the same group incorporated poly acrylic acid (PAA) into C-S-H[20] and reported intercalation of PAA as well as exfoliation of C-S-H. Their differential scanning calorimetry showed higher glass transition temperature of the hybrid material compared to the bulk polymer, thus suggesting potential applications in corrosive and high temperature environments.

It is widely hypothesized that in all polymer modified C-S-H nanocomposites, the material property enhancements arise primarily from the H-bonding between polymers and the layered structure of the C-S-H gel.[13,24] However, the underlying chemistry and physics of these interactions and the mechanisms of load transfer between polymers and C-S-H remain elusive.

3

The complexities originate from two major sources. First, polymers and C-S-H come from different chemistry classifications, thus unexpected characteristics can be found in their hybrid system which are absent in individual constituents.[25] The second source of complexity arises from the geometric anomaly between potential bonding agents at the interface of the two constituents, *i.e.* the short spacing distance between hydroxyl groups of PVA, compared to the longer spacing between silicon tetrahedra in the C-S-H substrate, . Therefore, a basic understanding rooted in the subatomic level could provide important fundamental chemical insights to introduce new design concepts and principles for *de novo* synthesis of advanced hybrid materials.

Herein, we report a combined first-principles calculations, molecular dynamics (MD) modeling and theoretical study that together elucidate the binding characteristics at the interface of PVA and silica chains of tobermorite mineral, a natural analog of C-S-H.[17] Tobermorite has a layered structure with three repeating units of silicon tetrahedra where the third unit, so-called bridging silicon tetrahedron, is slightly shifted up or down (Figure 1). Here, as our main intention is to provide a fundamental insight, the simulations are set up based on the assumption of basal intercalation, where PVA strands interact with the interlayer tobermorite silica chains. The intercalation of polymers and C-S-H is a function of C/S ratio and type of the polymer.[22] It is known that in the absence of interlayer (basal) intercalation, the composite behavior of the C-SH and polymers will be similar to that in traditional composites.[24] However, interlayer intercalation of polymers in stacked nanocomposites is an important step to achieve enhanced material properties. Experimental measurements report no increase in basal spacing of PVA interaction with C-S-H for C/S<1.[22] This suggests that interlayer intercalation of PVA does not occur for C-

4

S-H with C/S <1, and thus interactions are intralayer in nature. However, with no reported experimental results for 1.1nm tobermorite, the possibility of interlayer intercalation remains unknown. It must be noted that having intralayer or mixed intralayer-interlayer interactions adds more complexity to the environment.

First, by using potential mean force and time correlation function, we demonstrate that the H-bonding between hydroxyl groups of PVA and non-bridging oxygen atoms of silicate substrate are the primary source of adhesion at the interface of PVA-silicate system. Next, by pulling virtual experiments, we show that the effective resistance of the hybrid composite to fracture in shear mode is equivalent to fracture energy of approximately 2-6 H-bonds. This finding translates into the existence of an optimum overlap length for which the toughness (total elastic strain energy density) of the composite is maximized. To provide critical mechanistic insights on the sources of such optimized overlap length in hybrid materials, a general theoretical model is developed and validated by an atomistic size-effect study. Finally, the detailed mechanism of interfacial H-bonding network between the PVA and silicate substrate is demonstrated that is dictated by the geometric anomaly at the interface and intra-molecular H-bonding in PVA.

2 SYSTEM SET UP AND COMPUTATIONA PROTOCOLS

2.1 MD simulations. MD simulations were performed using a scalable parallel molecular dynamics simulator, LAMMPS.[26] The geometry of tobermorite crystal with a chemical formula of $Ca_6Si_6O_{18} \cdot 2H_2O$, was obtained from previous experimental work,[27] which includes 72 atoms per unit cell. The unit cell was then extended to a 1x7x1 supercell and relaxed with the CSH-FF

5

potential.[28] This potential is an improved version of CLAYFF[29] potential and has been obtained

by fitting to an extensive set of *ab-initio* data on C-S-H family.[28] The ability of CSH-FF potential

in accurately predicting the lattice parameters, bond distances and other higher order properties

of tobermorite and C-S-H has been previously validated against experiments or *ab-initio*

calculations.[28,30] Water molecules are modeled as the three-site simple point charge (SCP)[31] as

described in CSH-FF. Partial charges and cutoffs and all parameters of CSH-FF potential are

given in the supporting information (SI). The Consistent Valance Force Field (CVFF) potential[32]

is employed as interatomic potential for PVA. CVFF is previously used in predicting

hydrocarbon conformations and interface interactions.[33,34] The cross interaction terms between

PVA and tobermorite are computed based on the standard Lorentz-Berthelot combination rules.[35]

To study the interaction of PVA with tobermorite, a single PVA chain is placed on top of

a 1x7x1 supercell of tobermorite. The simulation was set up in this way to minimize the entropic

effects of polymer conformations and focus on the mechanical characteristics of the interface.

The PVA-tobermorite system is fully equilibrated in explicit water with approximate cell

dimensions of 25 Å × 105 Å × 40 Å and periodic boundary conditions in all directions (Figure

1). These dimensions are chosen such that the PVA and tobermorite do not interact with their

corresponding images. After relaxation, it turns out the parallel orientation of the PVA with silica

chains is the favorable orientation. The built-in steered molecular dynamics (SMD) tool of

LAMMPS was utilized to carry out the pulling virtual experiments. In our implementation, one

end of a linear spring is tethered to the terminal carbon atom of the PVA, while the other end is

pulled with a constant rate in either shear or tear direction, as shown in Figure 1. We used the

6

spring constant of K=10 kcal.mol^{-1}.Å^{-2} which has been previously used in similar computational

conformations.[36] A full study on the effect of the pulling rate is detailed in section 3.2
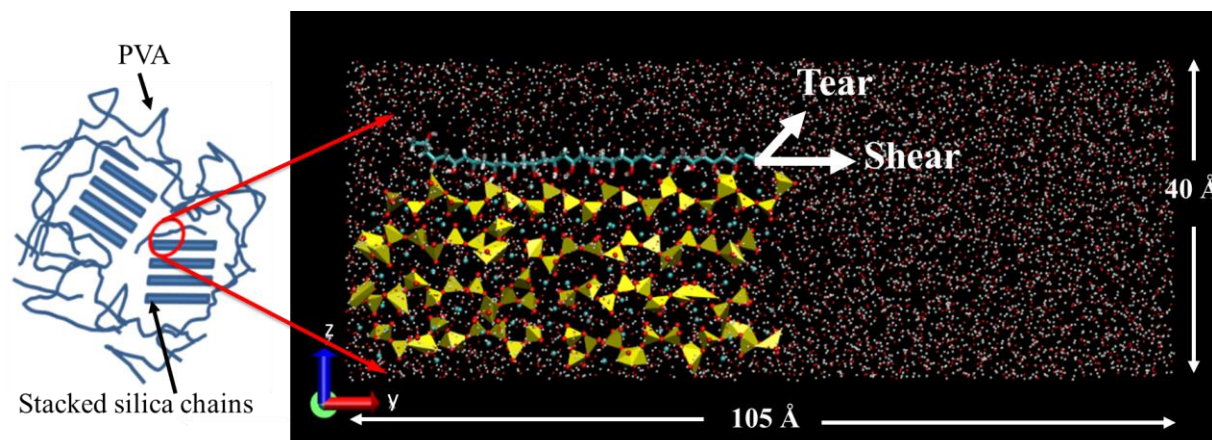
Figure 1 – A zoom at the interface domain of PVA and tobermorite substrate. In the full atomic

representation on the right, PVA chain is on the top and a silicate substrate (tobermorite) is at the

bottom. The PVA and silicates are surrounded by water molecules in a periodic simulation box.

In the shear mode, the polymer is dragged parallel to the silica chain of tobermorite while in the

tear mode, it is pulled normal to the axis of silica chains.

All MD relaxation and SMD simulations are performed under canonical ensemble (NVT)

at 300 K with Nose-Hoover thermostat[37,38] for the time integration. The simulations have been

relaxed for 2 ns with a time step of 1 fs and the trajectories are written out every 20 fs. To obtain

the mechanisms of H-bonding, a PVA chain with 18 monomers is dragged by SMD simulations

on tobermorite as shown in Figure 1.

2.2 DFT calculations. The geometries of representative PVA-silicate complexes are optimized

using density functional theory (DFT) with Becke's three-parameter hybrid functional combined

with Lee-Yang-Parr correlation functional (B3LYP) with 6-31+G* and 6-311++G** basis sets.[39]

The reliability of these methods in predicting the vibrational frequencies of H-bonded clusters is

7

confirmed earlier.[40] The geometries of all clusters were optimized on their respective potential

energy surfaces at the B3LYP/6-31+G* level of theory and atomic charge distributions are

calculated from natural bond orbital (NBO) analysis at B3LYP/6-311++G** level of theory.

Binding energies (BEs) of the complexes were calculated using the supermolecule approach and

corrected for basis set superposition error (BSSE) using the counterpoise (CP) procedure.[41]

Then, the BE is obtained *via*   where   is the total

energy of the complex and   and   are the PVA and tobermorite energies,

respectively. All calculations were performed using the Gaussian 09.[42]

3. RESULTS AND DISCUSSIONS

3.1 Classification of heterogeneous H-bonds in the PVA-silicate system. To obtain

information on the influence of the H-bonds on the interface interactions, it is necessary to define

them first. A hydrogen bond between a donor (*D*) and an acceptor (*A*) is usually defined based on

the energetic and/or geometric criteria. A widely used geometric criterion for a H-bond

symbolized by   – ··   is when $R < 3.5$ Å and   where R represents the distance between

   and   atoms, and   is the angle between the   –   and   –   rays.[43] While this criterion is

suited to describe H-bonds that form in bulk water, to reduce arbitrariness in defining H-bonds in

more complex systems such as PVA-tobermorite we adopt an energetic criterion based on two-

dimensional (2D) potential of mean force (PMF).[44] In this method, for each 2D PMF plot that is

constructed based on different choices of angles and distances, there is a lowest energy basin at

short distances. This basin corresponds to the H-bonded states and is detached by a saddle point

from another higher-energy basin that corresponds to the non-H-bonded states. Then, the

8

equipotential contour that passes through the saddle point delineates the boundary for the H-bond. Mathematically, the PMF,   , can be written as[44]

$$ \text{(1)} $$

where k_B is the Boltzmann constant, T is temperature, and   is the angular-radial distribution function defining the probability of finding an acceptor atom ( ) at the distance from the donor ( ) while forming an   angle of . In the PVA-tobermorite composite there are four different types of oxygen atoms: the oxygen of PVA (Op), the bridging oxygen of silicates (Ob), the non- bridging oxygen of silicates (Onb), and the water oxygen (Ow). While all of these oxygen atoms can serve as H-bond acceptors, Op and Ow can also function as H-bond donors.

To obtain PMF plots, the PVA chain is initially located parallel to the silica chains with a distance more than a typical H-bond length to prevent initial H-bonding (Figure 2a). After relaxation and investigating PMF plots for various pairs, it turns out there are only 7 types of H-bonds in our system, namely Op-Onb, Ow-Onb, Ow-Ob, Op-Op, Ow-Op, Op-Ow and Ow-Ow. In all these cases, the first symbols indicate the donor sites and the second symbols denote the acceptor sites. Figure 2b shows the PMF plots for these 7 cases calculated from MD simulations. The basins and saddle points are obvious in each PMF plot. To distinguish the heterogeneity of H-bonds strengths in the PVA-tobermorite system, we computed the intermittent H-bond Time correlation function (TCF)[30,43,45]

$$ \frac{\langle \qquad \rangle}{\langle \qquad \rangle} \qquad \text{(2)} $$

9

where $\langle \ \rangle$, and is a binary operator representing H-bond population variable that takes the value of one if a pair of donor and acceptor are H-bonded, and zero otherwise. The symbol $\langle \ \rangle$ denotes average over all the pairs and time origins.[46] $C(t)$ is a representation of the number of the pairs which remain H-bonded since the assigned reference time. Thus, for a perfectly H-bonded pair, $C(t)$ remains nearly one over time whereas deviations from one indicate weak H-bond interactions.

Considering H-bonds TCF in Figure 2c, the relaxation of the Op-Onb remains very slow even at long time scales, which indicates the high strength of this category of H-bonds. Note that Ow is in competence with Op to make H-bonds with Onb, however, Ow-Onb H-bond TCF decreases rapidly with time, indicating more favorable bonding between Op and Onb. Thus, we can conclude that Op-Onb H-bonds are the primary source of adhesion between PVA and silicates, serving as the load bearing points for load transfer between the organic and inorganic constituents of this hybrid composite.

10
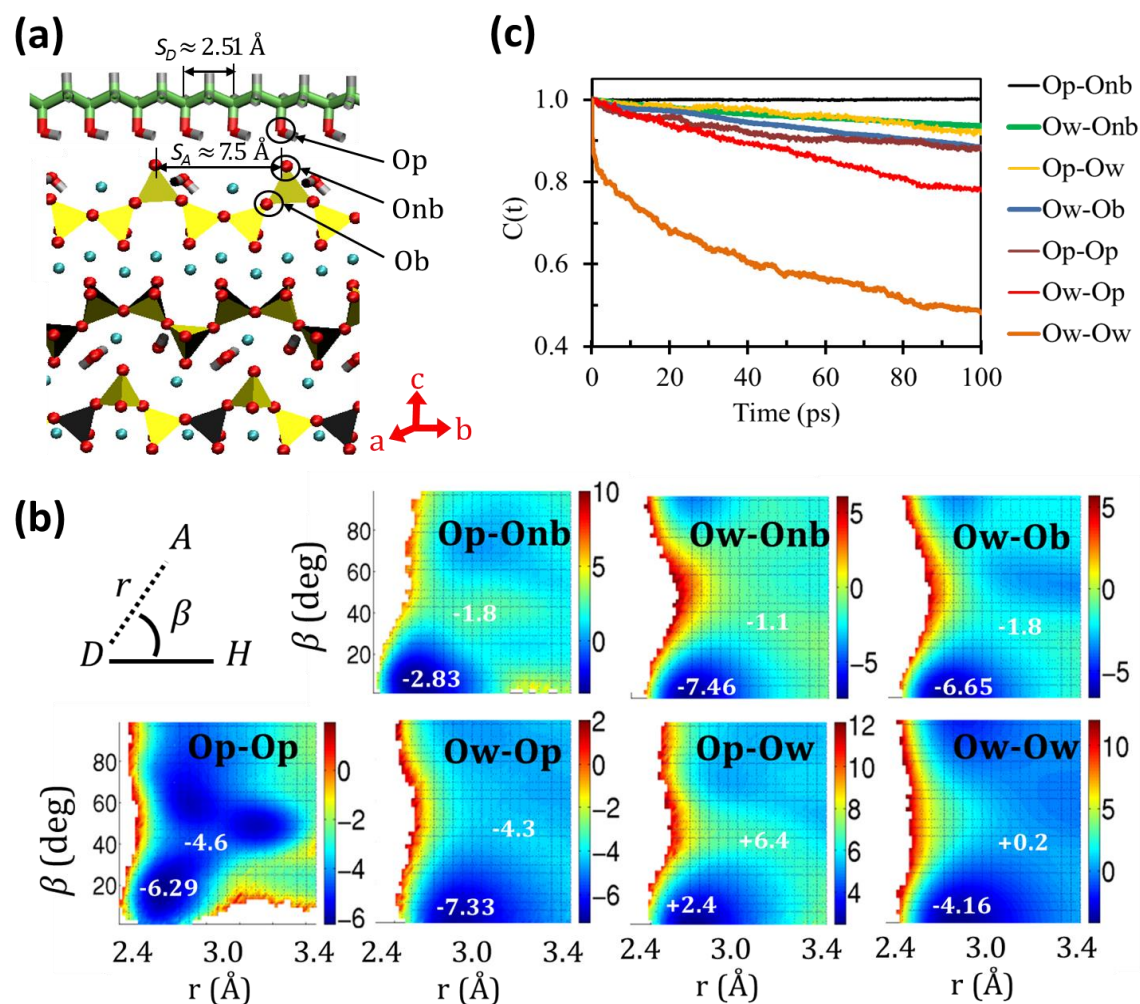
Figure 2 a) Close-up atomistic snapshot of the PVA-tobermorite interface. Silicon tetrahedra are shown in yellow, Oxygen atoms in red, Calcium atoms in cyan, Carbon atoms in green and Hydrogen atoms are shown in white. Op refers to oxygen of PVA, and Ob and Onb denote bridging and non-bridging oxygen atoms of silicates. b) Potential of mean force plots for possible H-bonds in the PVA-tobermorite system calculated from MD simulations. The contours in the color bar are in units of $k_B T$. In all cases the magnitude of the global minima and the saddle points are shown with a white color. The inset on the top-left shows a schematic picture of a H-bond denoted by an acceptor (A), donor (D) and the hydrogen atom (H). c) H-bond time correlation functions for different types of H-bonds. In the legend, the first and second atoms

11

separated by the dash line indicate the donor and acceptor sites, respectively. Op denotes oxygen of PVA, Ow oxygen of water, and Ob and Onb represent bridging and non-bridging oxygen atoms of silicates.

While the interfacial H-bonding (Op-Onb) will be the primary focus of the present work, we can rank all the hydrogen bonds from the strongest to the weakest as follows:

1) Op-Onb (oxygen of PVA/non-bridging oxygen of silicates)

2) Ow-Onb (water/non-bridging oxygen of silicates) and Op-Ow (oxygen of PVA/water)

3) Op-Op (oxygen of PVA/oxygen of PVA) and Ow-Ob (water/bridging oxygen of silicates)

4) Ow-Op (water/ oxygen of PVA)

5) Ow-Ow (water/water)

3.2 Efficient number of H-bonds cross-linking PVA and silicates. To quantitatively study the load transfer at the PVA-silicate interface, SMD simulations are performed to impose incremental strains until fracture of the interface. For this purpose, a PVA with 12 mers is dragged on the surface of the tobermorite. The pulling virtual experiments include both shear and tear modes. In both cases the PVA chain is initially equilibrated and placed in parallel to the silicate chains. Next, via SMD simulation, the force is applied in parallel (perpendicular) to the silicate chains in the shear (tear) mode (see Figure 1). We use the tear mode to study single H-bonds since they break sequentially and use shear mode to study clusters of H-bonds as they break simultaneously.[10]

12

To compute the required energy for H-bond breakage in shear and tear modes, modified Bell's theory[47] is utilized, which is an extension of the conventional Bell model[48] to relate bond associated properties with the pulling speed. In the modified Bell's theory, the rupture force scales linearly with the logarithm of pulling velocity[10] (Figure 3):

$$\frac{\quad}{\quad}\left(\quad - \quad\right) \quad \frac{\quad}{\quad} \tag{3}$$

$$\frac{\quad}{\quad} \qquad \frac{\quad}{\quad} \qquad\qquad \frac{\quad}{\quad} \tag{4}$$

In above,   is the reciprocal of the natural frequency of bond oscillation,   is the bond energy, F is the maximum applied force,   is the bond extension required to initiate fracture,   is the pulling velocity,   is the natural bond breaking speed,   is the temperature and   is the Boltzmann constant as before. For each shear and tear mode, we simulated pulling virtual experiments with several velocities from 0.3 to 50 m/s consistent with previous studies.[49,50] Next, by line fitting for the two unknowns,   , we calculated E_b and x_b (Figure 3b).

The energy barrier of the shear mode,   , corresponds to the fracture energy of a cluster of H-bonds and the energy barrier of the tear mode,

             , corresponds to that for a single H-bond. Thus, the ratio of indicates that an equivalent of nearly two H-bonds are broken simultaneously in the shear mode. In other words, under shear loading, regardless of how many H-bonds exist, the effective resistance to fracture is equivalent to fracture energy of a hybrid PVA-silicate system that is connected with ~2.1 H-bonds. Considering that each H-bond donor (hydroxyl group) of PVA is linked with exactly one monomer, *i.e.* 1 H-bond=1 monomer, this efficient number of H-bonds translates into an optimal overlap length that is critical for the shear load transfer and the overall

13

mechanical performance of the composite. Considering the length of each monomer   , the

modified Bell's theory suggest an optimum overlap distance of   for the chosen

system of PVA-tobermorite. The exact atomistic snapshots of H-bond assemblies before and

after shear failure are discussed in section 3.5.

(a)   **(b)**
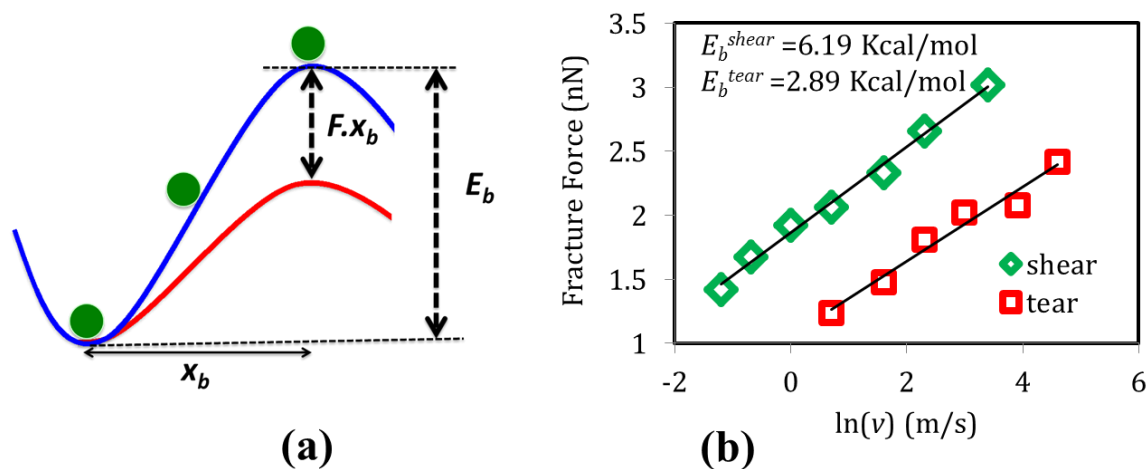
Figure 3. (a) Schematic profile of the energy barrier (E_b) and bond extension (X_b) between the equilibrium state and the transition state of an atomic bond. (b) SMD implementation of the modified Bell theory. The maximum forces for the shear and tear fracture modes are obtained as a function of the pulling speed, which after line-fitting result in estimation of energy barriers, E_b.

3.3 Shear load transfer between dissimilar building blocks: theoretical model. In the

previous section, the efficient number of H-bonds (overlap length) between the PVA and the

silica chain was investigated via MD simulations and relevant theories. In this section, a

theoretical-based model is proposed to reinforce the calculated overlap length and to provide

more fundamental insights on the shear load transfer between the polymer and the silica chain.

While the problem of shear load transfer between identical building blocks is studied within

14

1
2
3
4
5
6
7
8
9
10
11
12
13
14
15
16
17
18
19
20
21
22
23
24
25
26
27
28
29
30
31
32
33
34
35
36
37
38
39
40
41
42
43
44
45
46
47
48
49
50
51
52
53
54
55
56
57
58
59
60

different contexts including adhesive lap joints[51] and staggered materials,[52-54] to our knowledge there is no study on the details of the optimum overlap length between dissimilar building blocks (here PVA and silica chains). To address this issue and to better understand the details of load transfer between PVA and silicate, we construct a simple 2D theoretical model to study shear lag between tablets with dissimilar properties and dimensions.

Assume two connected tablets with Young moduli, E_1 and E_2 and widths of b_1 and b_2 subjected to stress   on the right end of the top tablet (Figure 4a). Additionally, the system is clamped at the left end of the bottom tablet, and traction-free on all other dimensions except the overlap length, L. In our particular example, the top tablet denotes the PVA chain and the bottom tablet corresponds to the silica chain. The model also includes an intermediate layer (with thickness h), which models the interfacial H-bond layer between the PVA and the silica chains. The theoretical approach is derived in full detail in the Supporting Information (SI). We find that

$$-\left[\rule{6cm}{0pt} \right]$$

$$\rule{1.5cm}{0pt}\left[\rule{6cm}{0pt} \right] \qquad (5a\text{-}c)$$

$$\left(\rule{1cm}{0pt} \rule{1cm}{0pt} - \left[\rule{4cm}{0pt} \left(\rule{1cm}{0pt} \right) \right] \right.$$

where

$$- \qquad - \qquad\qquad\qquad - \qquad\qquad (6)$$

In above,   and   are the axial stresses on the top and bottom tablets,   is the shear stress between the two tablets, G and h are the shear modulus and thickness of the interface, respectively. The elastic solutions expressed above are the generalized solution to the shear-lag

15

problem of identical tablets and dimensions.[55-57] For the PVA parameters of

,[58] and tobermorite parameters of ,[59] (hence $m=0.3$, $n=1.885$)

the typical axial and shear stress distributions are shown in Figure 4b,c. Compared to the two

ends of the overlap length, the central region not carry much shear load, and thus is expected to

contribute minimally to the overall strength of the hybrid system. Non-uniform but symmetric

distribution of shear stress in staggered layer composites or shear lag models is known.[51,56,57]

However, our model reveals that for dissimilar tablets shear stress distribution is not symmetric.

In other words, not only the contribution of the interfacial H-bonds in the central region is

negligible to the shear load transfer, but also those at the left end bear less shear stress compared

to the H-bonds on the right end (Figure 4b). Note that while these behaviors may slightly change

by choosing different estimates of from the literature, the general trends of the plots in

Figure 4 are unchanged.

To quantify influence of shear and axial stresses on rupture, we focus on the elastic strain

energy density as it directly relates to the toughness and failure force. Toughness is a key

material property that describes the ability of the material to adsorb energy and deform without

fracturing. For a material with a brittle interface failure such as PVA-silicate, the toughness is

identical to the total elastic strain energy density, W_{total}. This parameter for the composite in

Figure 4a can be written as (see SI)

$$- \overline{\qquad} \tag{7}$$

where

$$\frac{(\quad)(\quad (-))}{16} \tag{8}$$

Equation (7) indicates that for fixed material properties of the composite, (, G) and

constant thicknesses of the matrix and tablets (h,   ), *i.e.* constant m and k, the toughness

is only the function of the overlap length, L. Thus, to maximize toughness, one has to maximize

        . By using $m=0.3$ and $n=1.885$ for the PVA-tobermorite composite, the maximum of

        occurs   at   ,   suggesting   an   optimum   overlap   length   of

$$\sqrt{\rule{1.5cm}{0pt}}$$ where h and G are taken 3   and $G=8.2$ GPa, respectively (see SI).

Considering the approximate length of each PVA monomer 2.51   this optimum overlap length

of 14.6   yields   as the optimum number of H-bonds (monomers), which is quite

comparable with the modified Bell's theory predictions (   ). Given

the idealized nature of the 2D theoretical model compared to the atomistic simulation, this level

of agreement in the order of magnitude is quite encouraging. The differences mainly arise from

the complex processes that exist in the atomistic simulations but not accounted for in the

theoretical model. These include the drag force of the surrounding water molecules on PVA in

the pulling processes, various H-bonding between different species (as discussed in section 3.1)

that may dynamically change the PVA adhesion to substrate and so on.
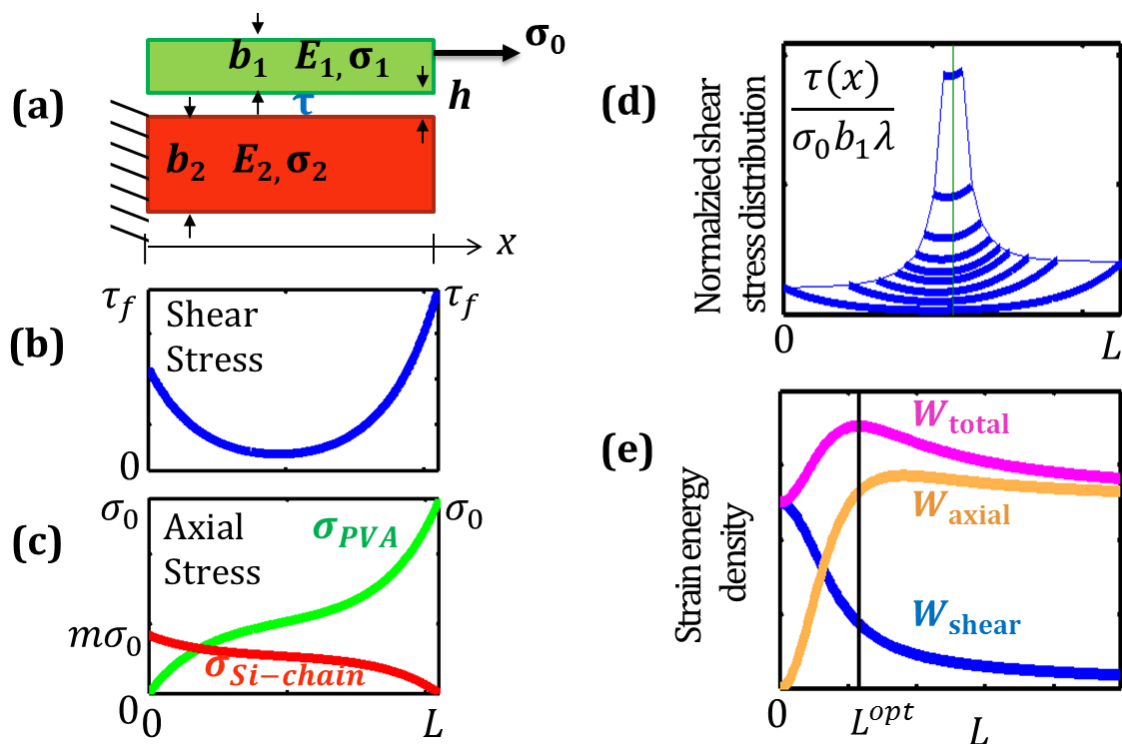
17

Figure 4. Analytical results of the elastic solution to the system of two dissimilar tablets under shear load interacting via a soft matrix. a) Schematic view of the hybrid system where the top and bottom tablets represent PVA and Si-chain, respectively. b) typical shear stress distribution across the interface. c) typical axial stress distributions in the top and bottom tablets. d) Normalized shear stress distribution as a function of varying overlap length. Note the higher values for shorter overlap length. e) The behavior of total elastic strain energy density (toughness) and its shear and axial components as a function of the overlap length ($W_{total} = W_{axial} + W_{shear}$). At an optimum overlap length, the toughness W_{total} is maximized.

Figures 4d and 4e show respectively the typical shear stress distribution, eq (5c), across the interface, and strain energy density (toughness) components obtained from the theoretical predictions as a function of the overlap length, L. It turns out that both the average shear stress, $^{-}$

as well as the shear component (W_{shear}) of the total strain energy density increase by decreasing

L. These changes are even more pronounced for small overlaps where both   and W_{shear}

approach their maximum values at the asymptotic limit of zero overlap length. However, at this

extreme limit, the contribution of axial strain energy density W_{axial} (combined contributions from

PVA and Si-chain) to total strain energy approaches zero. Thus, there is an optimum overlap

length in which both shear and axial stresses offer their best contributions to maximize overall

toughness W_{total} (Figure 4e). Note that the overlap length in which W_{total} is maximized is different

than where W_{axial} is maximized. In our system, W_{axial} indicates contribution of intra-layer bonds in

both PVA and silicate layers to W_{total} while W_{shear} represents contribution of the inter-layer H-

bonds between PVA and silicates W_{total}. For a hybrid material with a brittle interface (linear

elastic shear until failure) such as PVA-silicate, W_{total} reaches to its final value prior to failure.

Thus, by varying the overlap length, one may find an optimum overlap length for which W_{total} is

maximized preceding the interfacial failure. Note that here due to the stiff covalent C-C and Si-O

bonds in PVA and silicates, upon pulling PVA on silicate substrate, mainly the angular C-C-C

bond in PVA increase to accommodate the imposed intra-layer stress. Our results show that the

average C-C-C angle in PVA changes from   109° in equilibrium state to   112° preceding

interfacial H-bond failure under shear mode.

Hence, although counterintuitive, at the optimum overlap length, the intra-layer angular

bonds in PVA and silicates slightly stretch to maximize overall toughness W_{total} preceding the

inter-layer (interfacial) H-bond failure. In fact, this is what the modified Bell's theory predicts

from atomistic standpoint for brittle bond fracture. In such cases, the rupture force and maximum

elastic strain energy density occur simultaneously. This analysis clearly explains the sources of

19

the limited number of H-bonds (*i.e.* optimum overlap length) from the absorbed energy standpoints in the intra- and inter-layer bonds. The fact that the results of this model only depend on intrinsic, "first-principles" properties of PVA and tobermorite and their geometry underlines the significance of our finding.

We can employ the elastic solution presented so far to infer about the failure force and the average interfacial shear strength of the hybrid material as a function of the overlap length. Considering that the brittle interface collapses at shear strength,   , by rearranging eq (5c), one can obtain the failure force of the composite for a unit lateral length as

$$\overline{\qquad \qquad \qquad \qquad \qquad}$$ (9)

This equation indicates that the failure force,   initially increases with the overlap length and then becomes saturated. But the average interfacial shear strength, $\overline{\quad} - \dfrac{\int \quad}{\qquad}$,

decrease with the overlap length. These two behaviors (not the magnitudes) are both independent of the choice of the material properties (and dimensions (b_1, b_2, h). This rigorous theoretical derivation is strongly supported by an atomistic size-effect study described next.

3.4 Atomistic size-effect study on the influence of overlap length. We performed the size-effect study *via* SMD simulations by repeating the pulling virtual experiment in the shear mode for a PVA with chain lengths extending from one up to twelve monomers (Figure 5). The speed of pulling was fixed at 5×10^{-6} femtosecond/Å, consistent with previous studies.[36] To minimize the effects of initial configuration of PVA on the substrate, several simulations with

20
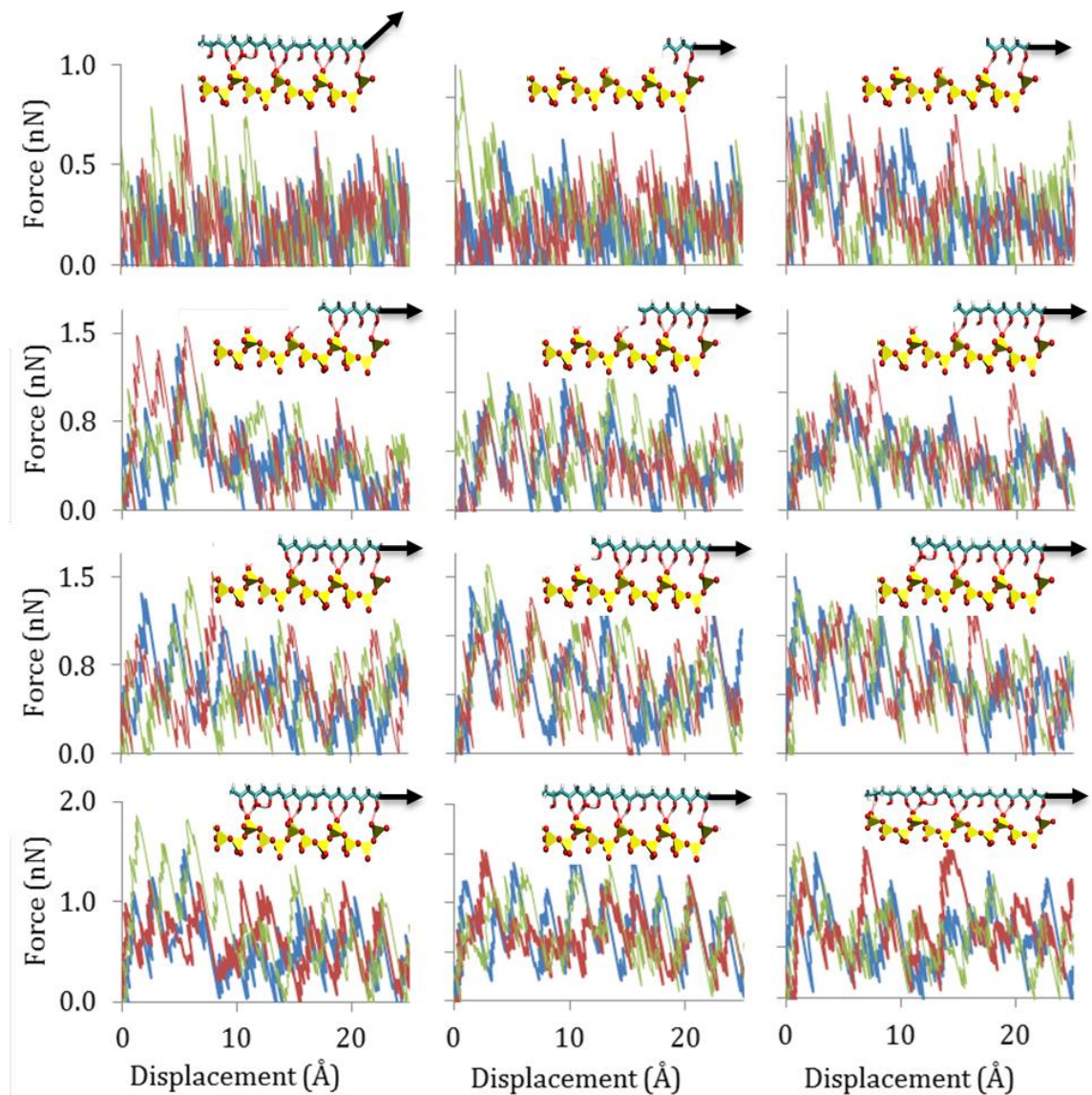
Figure 5. Atomistic size-effect study by SMD simulations to predict the failure force for different overlap lengths in PVA-silicate system. Twelve cases are considered representing overlap lengths of 1 to 12 mers. Note that in the top-left panel, the computational pulling is conducted out of the plane to break single H-bonds, *i.e.* tear mode. All other pulling experiments demonstrate the shear mode. The colors in each panel denote SDM results corresponding to different initial conditions.

21

different initial positions were conducted to obtain the average values of failure force from the first peak of force-displacement plots. Note that in the tear mode (the top-left panel in Figure 5), the pulling direction is out of the plane to break single H-bonds representing the failure force for a single mer.

Figure 6a and 6b represent respectively the failure force and the average interfacial shear strength obtained from the SMD simulations and theoretical model as a function of the number of monomers (overlap length). The trend obtained from the SMD simulations matches very well with our theoretical predictions. Together, they demonstrate that i) the failure force of the composite initially increases linearly and then becomes saturated at an overlap length that is much larger than L^{opt} for which the toughness was optimized, and ii) the average interfacial shear strength monotonically increases by decreasing the overlap length. This latter finding obtained from rigorous mathematical modeling and a systematic size-effect study by atomistic simulations has a significant physical meaning: it elucidates that in contrast to the current understanding and reports that correlate maximum "shear strength" with rupture of interfacial H-bonds assemblies at optimum overlap lengths, *e.g.* -sheets in spider silks,[10-12] we find that the maximum toughness incorporating both axial (intra-layer) and shear (inter-layer) strain energy densities governs the rupture of interfacial H-bond assemblies at the optimum overlap length. This universally valid result, which is independent of the choice of natural or synthetic materials and geometric dimensions, is the most significant result of our paper. In the PVA-silicate system, the maximum toughness mainly comes from intra-layer contributions (C-C-C angular bonds in PVA and Si-O-Si bonds in silicates) and inter-layer H-bond contributions (Op-Onb H-bonds). It should be noted that the relatively large values of shear stress in Figure 6b is due to the very

22

small overlap area (length of less than ~30 Å, and unit lateral thickness) considered here.

Nevertheless, the trends of the results are independent of the dimensions.
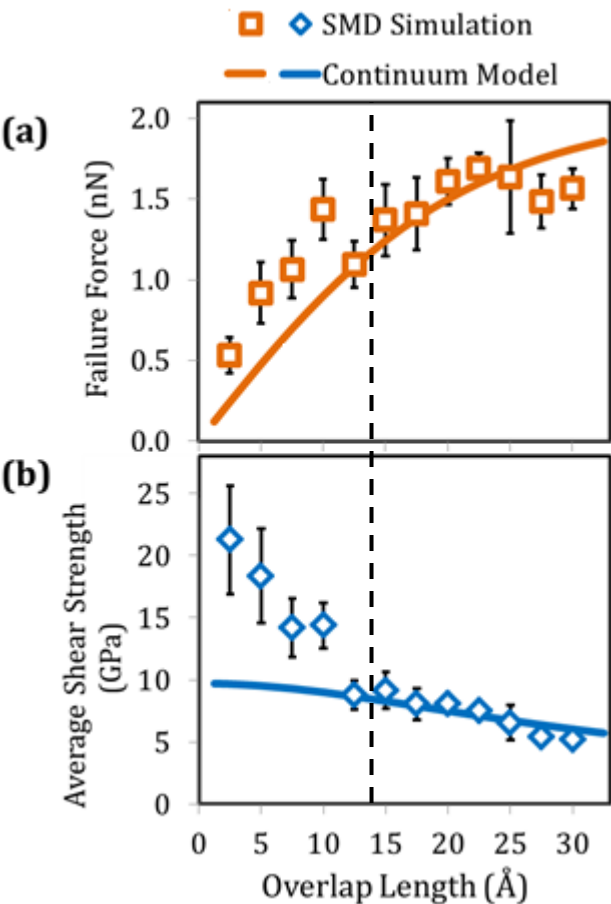
Figure 6. The failure force and the average interfacial shear strength of the hybrid material as a function of the overlap length (number of monomers). Both the theoretical model and the atomistic size-effect study show that the failure force increases monotonically as a function of the overlap length until it becomes saturated (a). The average interfacial shear strength is only maximized at the limit of zero overlap length (b). This confirms that unlike the earlier results in the literature (e.g. H-bonded -sheet systems in proteins), the maximum shear strength cannot explain the sources of the optimum overlap length (see text). The vertical bars in (a-b) show the

23

error bars in SMD simulations. The dashed line represents the location of the optimum toughness predicted by the continuum analysis.

Note that an efficient overall load transfer occurs at an overlap length where the highest toughness and strength are met simultaneously. This is what happens in nature materials such as nacre, making them strong and tough concurrently. In the case of PVA-tobermorite, our continuum model predicts that toughness is maximized at   while the strength will be asymptotically increasing with length. At   the strength will reach 90% of its saturation value (see SI). Therefore, strength is optimized at an overlap length that is about 57% more than the length scale where toughness is maximized. Better efficiency can be achieved by tuning the tablet (tobermorite and/or PVA) and the interface (H-bonds) properties, e.g. use of another type of polymer such that the two length scale get closer. This will be discussed in detail in the future.

It is worthwhile to mention that our theoretical model is derived in a general framework that provides fundamental physical intuitions useful to understand, conceptualize and introduce new design concepts and principles for complex systems such as hybrid organic-inorganic materials with dissimilar building blocks.

3.5 Basic mechanisms of H-bonding at the PVA-silicate interface. The atomistic and theoretical results discussed so far provide the basic mechanistic insights on how H-bonding across the interface (particularly at the two ends) contributes to the load transfer and the optimized overlap length in hybrid materials. In this section, we unravel the detailed mechanisms

24

of the H-bond rupture and formation that are key to load transfer at the interface of PVA and silica chains. The slip-stick behaviors of shear force versus displacement in Figure 5 indicate successive H-bond breakage and reformation. Additionally, the individual sudden force drops represent a brittle fracture behavior at the interface (although the overall saw-tooth process may be viewed as a flaw-tolerant or may imply a deformation mode similar to those in metallic glasses[60] or glassy polymers[61]). As observed in a typical SMD simulation of Figure 5 (see the movie in SI) and illustrated schematically in Figure 7, the distance between H-bond donor sites, S_D, and acceptor sites, S_A, are such that they dictate a certain H-bonding mechanism. Specifically, for every three adjacent hydroxyl groups of PVA (named as **1**,**2**,**3**), two are H-bonded to a common acceptor site (Onb) in the substrate while the third one does not participate in any inter-molecular H-bonding. Given such a geometric pattern, the detailed slip-stick processes in the PVA-silicate system include three basic mechanisms, which occur almost simultaneously. The first mechanism is the breakage of H-bond **1**, which is immediately followed by (or concurrent with) the second mechanism, that is, shifting of H-bond **2** from an old alignment in Figure 7a to a new one in Figure 7c. This H-bond does not break during this reconfiguration. The third mechanism is the formation of a new H-bond **3**, which was not H-bonded previously and is formed in lieu of the broken H-bond **1** (Figure 7c).
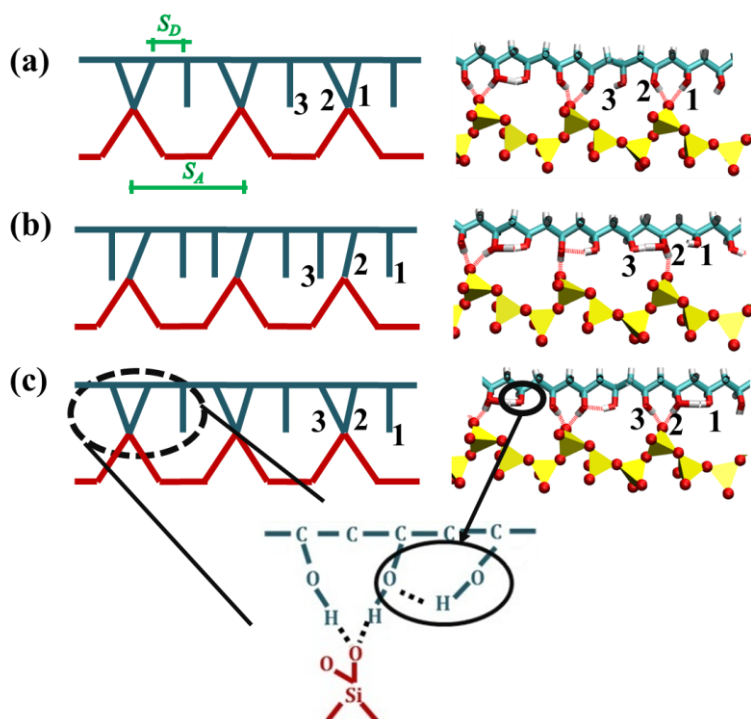
25

Figure 7. Detailed atomistic mechanisms of slip-stick processes between PVA and silicate substrate under shear force. (a-c) the schematic pictures on the left hand side represent the inter-molecular H-bonds shown on the right hand side, obtained from the snapshots of SMD simulations. a) PVA is shown on the top of the silica chain where two donor sites (two Op) share a common acceptor (Onb). On the left, each line in the PVA represents a hydroxyl group. b) rupture of H-bond **1,** followed by reconfiguration of H-bond **2.** c) The formation of a new H-bond **3** to recover the initial arrangement in (a). The dashed black circle on the left highlights in the inter- and intra-molecular H-bonding while the solid black circle on the right represent a typical intra-molecular H-bonding in PVA. Flanked Si atoms of the substrate have two attached oxygen atoms but only one of them acts as a host site for inter-molecular H-bonding to PVA (the other oxygen atom is out of plane and has a larger distance to the donor site). In b) to c) red and white colors represent oxygen and hydrogen atoms while silicon and carbon atoms are shown with yellow and cyan colors. The dashed lines denote H-bonds.

26

While these basic mechanisms are identical for all the repeating units of the PVA-silicate interface, there are instances where local intra-molecular H-bonding may significantly influence the interfacial properties. In particular, depending on the travelled distance of the PVA chains and the local environment, there might be intra-molecular Op-Op H-bonding in the PVA. This is due to the mismatch distance between the donor and acceptor sites (at the interface. As shown in Figure 7c, the hydroxyl groups of the PVA chain, which cannot find any host at the silicate substrate, may form intra-molecular H-bonds to acceptors within their own adjacent hydroxyl groups. To reveal the influence of these relatively strong H-bonds (see Figure 2c for comparison of H-bond strengths) that form within the PVA molecule on the interfacial mechanics of the hybrid PVA-silicate system, we performed first-principles calculations with high level of theory on small systems of PVA and silicon tetrahedra. Two cases were considered:

1) a PVA with an intra-molecular H-bonding, and

2) a PVA without an intra-molecular H-bonding.

In both cases, the PVAs interact with a silicon tetrahedron (Figure 8). Table 1 shows the calculated stretching frequency, intensity, red shift values and binding energies of the complexes for these two cases. Vibrational spectroscopy is a valuable tool to quantify the strength of weak H-bonding interactions in various complex materials. The free O-H stretching frequencies prior to complex formation in case 1 and 2 are 3655 and 3649 cm^{-1} and after the complex formation, these values change to 3277, and 3373 cm^{-1}, respectively. The calculated O-H frequency of case 1 is consistent with available experimental data,[62] *i.e.* 3250 cm^{-1}. The corresponding red shift and intensity values of Table 1 suggest that the case 1 has a better inter-molecular connectivity than case 2. This can be verified from the calculated binding energy (BE) and electronegativity of

27

atoms influencing the interfacial bonding (Figure 8). The BE of the complex in the case 1 is approximately 4 kcal/mol larger than that of in the case 2. Considering the electronegativity of atoms, before complex formation the charges on the oxygen atoms in PVA are less negative compared to those after complex formations. This reveals that electrons transfers from the Si-O bond to the H-O bond when a H-bond is formed. Particularly in case 1 (Figure 8b), due to the intra-molecular H-bonding of PVA, the charge transfer is higher than that in the complex in case 2 (Figure 8d). This results in shorter H-bond distances and thus stronger inter-molecular H-bonding across the interface. Interestingly, upon complex formation the intra-molecular H-bonding of PVA, i.e. Op-Op, become shorter and stronger too (cf. Figure 8a and 8b).

Overall this analysis clearly elicits that intra-molecular H-bonding in the PVA moiety, *i.e.* Op-Op, play a crucial role in the PVA-silicate complex formation and increase the strength of the inter-molecular Op-Onb H-bonds across the interface. This suggests that the use of polymers with more intra-molecular H-bonding may result in more interfacial adhesion, a feature that is not intuitive. This is particularly important for improving the synthetic brick-and-mortar composites (e.g. soft organic matrix with reinforcing inorganic platelets) discussed in section 1. Moreover, the first-principles analyses show that the PVA-silicate complexes are predominantly stabilized by the inter-molecular H-bonds between PVA and silicates (Op-Onb), corroborating our results inferred from the PMF plots.

Finally, although PVA-silicate building blocks were used in this study as a platform to provide fundamental insights and quantitative mechanistic information on the interface interactions generated through a complex H-bond network, our findings have important

28

implications on several other hybrid materials made of dissimilar building blocks in both natural
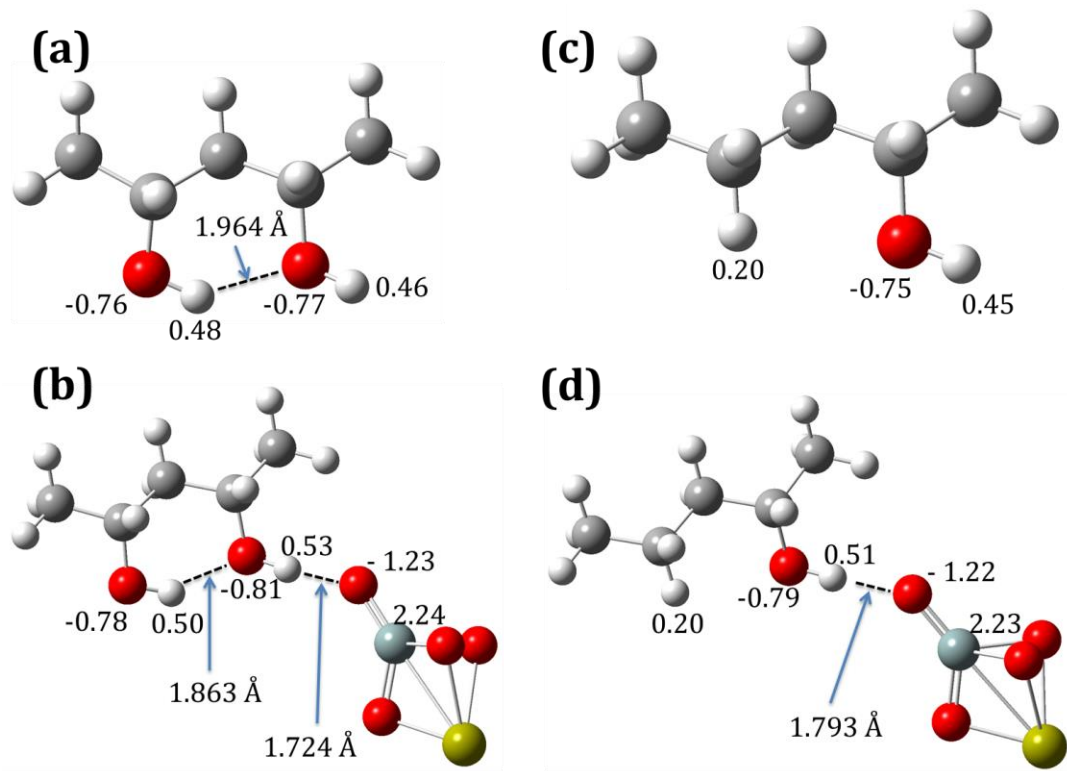
and synthetic systems.

Figure 8. (a) and (b) show optimized geometries and atomic charge distributions of a PVA with an intra-molecular H-bond before and after complex formation with a silicon tetrahedron, respectively. For clarity only partial charges close to the interface are shown. (c) and (d) show optimized geometries and atomic charge distributions of a PVA without an intra-molecular H-bond before and complex formation with a silicon tetrahedron, respectively. For clarity only partial charges close to the interface are shown. The data are obtained from the B3LYP/6-311++G** level of theory. The grey, white and red spheres represent carbon, hydrogen and oxygen atoms respectively, and orange and dark red denote silicon and calcium atoms. The calcium atoms are added to ensure charge neutrality.

29

Table 1. Calculated O-H stretching frequencies, red shifts and binding energies of PVA-silicate complexes at B3LYP/6-31+G* Level of theory, along with available experimental value (cm^{-1}).

PVA/silicate Complex	O-H Stretching	ν_{cal} (cm^{-1})	Intensity	Red Shift (cm^{-1})	ν_{exp} (cm^{-1})	BEs (kcal/mol)
PVA **Case 1:**	Free O-H	3655	20			
	Intra-molecular H-bond	3581	157			
PVA-silicate	O–H…O$_S$	3277	1716	378	3250	14.47
	Intra-molecular H-bond	3460	273	121		(13.90)^a
PVA **Case 2:**	Free O-H	3649	20			
PVA-silicate	O–H…O$_S$	3373	1201	276		10.60 (9.73)

^{a} BEs calculated at B3LYP/6-311++G** level.

4. CONCUSIONS

In summary, we conducted a suite of DFT calculations, MD simulations and theoretical methods to study the basic atomistic interactions, deformation mechanisms and failure events of PVA-silicate systems, as an example of hybrid materials with geometric and material property mismatch across the interface. Our results reveal that the inter-molecular H-bonding between PVA and the non-bridging oxygen atoms of the silicate substrate are the primarily source of adhesion and load transfer in such hybrid materials. This H-bond assembly has a certain periodic pattern controlled by the interfacial geometric anomaly. Specifically, due to the mismatch between successive donors and acceptor sites, for every three hydroxyl groups of PVA, two are H-bonded to a single acceptor site in silicate substrate while the third hydroxyl group is left non-bonded. However, depending on the applied force and local environment, these standalone

hydroxyl groups may form intra-molecular H-bonding within PVA, which then entail non-intuitive consequences: intra-molecular H-bonding within PVA increases the electronegativity of atoms that are participating in the inter-molecular H-bonding, thus resulting in larger binding energy and adhesion across the interface. The latter suggests that depending on the frequency of host-sites, the use of polymers with possibility of more intra-molecular H-bonding may result in better mechanical adhesion to the substrate. This is particularly important for improving the connectivity of synthetic brick-and-mortar composites (e.g. inorganic reinforcing platelets embedded in a soft organic matrix).

More importantly, we developed a general theoretical model that formulated the deformation of two dissimilar tablets connected by a soft matrix. By linking the results of modified Bell's theory and theoretical derivations, we find that the maximum toughness, incorporating both axial (intra-layer) and shear (inter-layer) strain energy contributions, governs the existence of optimum overlap length and thus the rupture of interfacial H-bond assemblies in natural and synthetic materials. This universally valid result is in contrast to the current understanding and reports that correlate "shear strength" with rupture of H-bonds assemblies at optimum length scales.[10-12] We demonstrated that at the optimum overlap length, the intra-layer bonds in in the tablets slightly stretch to maximize toughness W_{total} preceding the inter-layer (interfacial) H-bond failure. The developed theoretical model is not limited to the PVA-silicate materials and can be used for numerous organic, inorganic or hybrid materials.

Our results may lay the foundation for the development of new "unit processes" that govern the rupture of hybrid organic-inorganic materials. A rich set of models for the deformation and fracture of ceramics and metallic systems have been developed over the past

31

decades, describing dislocations, shear bands and plasticity. However, similar advances for hybrid organic-inorganic materials, especially at their interface which is often the roadblock for improving the material properties, have thus far remained elusive. In analogy to dislocation nucleation and propagation in metals or shear band in metallic glasses, the breaking of interfacial H-bonds across the interface represents a basic unit process of failure in hybrid organic-inorganic materials. To the best of our knowledge, this report for the first time describes a rigorous holistic approach integrating DFT calculations, MD simulations, size-effect study and theoretical methods to describe the fundamental deformation mechanisms and interfacial H-bond failure events in hybrid organic-inorganic materials.

SUPPORTING INFORMATION

Complete derivation of the theoretical model, extraction of shear modulus (G) and maximum shear strength (, CSH-FF force field potential parameters, a 2 ns movie of SMD simulation of pulling PVA on silicate substrate representing the slip-stick motions. In the movie, the successive breakage and formation of H-bond assemblies are clearly visible. This material is available free of charge via the Internet at http://pubs.acs.org.

ACKNOWLEDGEMENT

32

REFERENCES

1.   Espinosa, H. D.; Rim, J. E.; Barthelat, F.; Buehler, M. J., Merger of structure and material in nacre and bone – Perspectives on de novo biomimetic materials. *Progress in Materials Science* **2009,** 54, (8), 1059-1100.

2.   Fratzl, P.; Burgert, I.; Gupta, H. S., On the role of interface polymers for the mechanics of natural polymeric composites. *Physical Chemistry Chemical Physics* **2004,** 6, (24), 5575-5579.

3.   Gao, H., Application of Fracture Mechanics Concepts to Hierarchical Biomechanics of Bone and Bone-like Materials. *Int J Fract* **2006,** 138, (1-4), 101-137.

4.   Beaudoin, J.; Dramé, H.; Raki, L.; Alizadeh, R., Formation and properties of C-S-H–PEG nano-structures. *Materials and Structures* **2009,** 42, (7), 1003-1014.

5.   Bonderer, L. J.; Studart, A. R.; Gauckler, L. J., Bioinspired Design and Assembly of Platelet Reinforced Polymer Films. *Science* **2008,** 319, (5866), 1069-1073.

6.   Rexer, J.; Anderson, E., Composites with planar reinforcements (flakes, ribbons)—A review. *Polymer Engineering & Science* **1979,** 19, (1), 1-11.

7.   Tang, Z.; Kotov, N. A.; Magonov, S.; Ozturk, B., Nanostructured artificial nacre. *Nature Material* **2003,** 2, (6), 413-418.

8.   Medhekar, N. V.; Ramasubramaniam, A.; Ruoff, R. S.; Shenoy, V. B., Hydrogen Bond Networks in Graphene Oxide Composite Paper: Structure and Mechanical Properties. *ACS Nano* **2010,** 4, (4), 2300-2306.

33

9.   Compton, O. C.; Cranford, S. W.; Putz, K. W.; An, Z.; Brinson, L. C.; Buehler, M. J.; Nguyen, S. T., Tuning the Mechanical Properties of Graphene Oxide Paper and Its Associated Polymer Nanocomposites by Controlling Cooperative Intersheet Hydrogen Bonding. *ACS Nano* **2011,** 6, (3), 2008-2019.

10.   Keten, S.; Buehler, M. J., Geometric Confinement Governs the Rupture Strength of H-bond Assemblies at a Critical Length Scale. *Nano Letters* **2008,** 8, (2), 743-748.

11.   Keten, S.; Buehler, M. J., Strength limit of entropic elasticity in beta-sheet protein domains. *Physical Review E* **2008,** 78, (6), 061913.

12.   Keten, S.; Xu, Z.; Ihle, B.; Buehler, M. J., Nanoconfinement controls stiffness, strength and mechanical toughness of [beta]-sheet crystals in silk. *Nat Mater* **2010,** 9, (4), 359-367.

13.   Beaudoin, J. J.; Raki, L.; Alizadeh, R., A 29Si MAS NMR study of modified C–S–H nanostructures. *Cement and Concrete Composites* **2009,** 31, (8), 585-590.

14.   Matsuyama, H.; Young, J. F., Synthesis of calcium silicate hydrate/polymer complexes: Part I. Anionic and nonionic polymers. *Journal of Materials Research* **1999,** 14, (8), 10.

15.   Minet, J.; Abramson, S.; Bresson, B.; Franceschini, A.; Van Damme, H.; Lequeux, N., Organic calcium silicate hydrate hybrids: a new approach to cement based nanocomposites. *Journal of Materials Chemistry* **2006,** 16, (14), 1379-1383.

16.   Pellenq, R. J.-M.; Lequeux, N.; Van Damme, H., Engineering the bonding scheme in C-S-H: The iono-covalent framework. *Cement and Concrete Research* **2008,** 38, 159-174.

17.   Taylor, H. F. W., Proposed Structure for Calcium Silicate Hydrate Gel. *Journal of the American Ceramic Society* **1986,** 69, (6), 464-467.

18.   Alizadeh, R. Nanostructure and engineering properties of basic and modified calcium-silicate-hydrate systems University of Ottawa, 2009.

19.   Okamoto, M. *Polymer/layered silicate nonmcomposites*; Rapra Technology Ltd: 2003; p 166.

20.   Mojumdar, S. C.; Raki, L., Synthesis, thermal and structural characterization of nanocomposites for potential applications in construction. *Journal of Thermal Analysis and Calorimetry* **2006,** 86, (3), 651-657.

21.   Sinha Ray, S.; Okamoto, M., Polymer/layered silicate nanocomposites: a review from preparation to processing. *Progress in Polymer Science* **2003,** 28, (11), 1539-1641.

22.   Matsuyama, H.; Young, J. F., Intercalation of Polymers in Calcium Silicate Hydrate: A New Synthetic Approach to Biocomposites? *Chemistry of Materials* **1998,** 11, (1), 16-19.

23.   Merlin, F.; Lombois, H.; Joly, S.; Lequeux, N.; Halary, J.-L.; Van Damme, H., Cement-polymer and clay-polymer nano- and meso-composites: spotting the difference. *Journal of Materials Chemistry* **2002,** 12, (11), 3308-3315.

24.   Mojumdar, S. C.; Raki, L., Characterization and properties of calcium silicate hydrate polymer nanocomposites. In *Proceedings of The American Ceramic Society 107th Annual Meeting*, 2005; pp 1-10.

25.   Chujo, Y., Organic-Inorganic Nano-Hybrid Materials. *Kona: Powder and Particle Journal* **2007,** 25, 255-260.

26.   Plimpton, S., Fast Parallel Algorithms for Short-Range Molecular Dynamics. *Journal of Computational Physics* **1995,** 117, (1), 1-19.

35

27.   Hamid,   S.   A.,   The   crystal   structure   of   the   11Å   natural   tobermorite Ca2.25[Si3O7.5(OH)1.5] · 1H2O. *Zeitschrift für Kristallographie - Crystalline Materials* **1981,** 154, (3-4), 189-198.

28.   Shahsavari, R.; Pellenq, R. J. M.; Ulm, F.-J., Empirical force fields for complex hydrated calcio-silicate layered materials. *Physical Chemistry Chemical Physics* **2011,** 13, (3), 1002-1011.

29.   Cygan,   R.   T.;   Liang,   J.-J.;   Kalinichev,   A.   G.,   Molecular   Models   of   Hydroxide, Oxyhydroxide, and Clay Phases and the Development of a General Force Field. *The Journal of Physical Chemistry B* **2004,** 108, (4), 1255-1266.

30.   Youssef, M.; Pellenq, R. J. M.; Yildiz, B., Glassy Nature of Water in an Ultraconfining Disordered Material: The Case of Calcium−Silicate−Hydrate. *Journal of the American Chemical Society* **2011,** 133, (8), 2499-2510.

31.   Teleman,   O.;   Jönsson,   B.;   Engström,   S.,   A   molecular   dynamics   simulation   of   a   water model with intramolecular degrees of freedom. *Molecular Physics* **1987,** 60, (1), 193-203.

32.   Cornell, W. D.; Cieplak, P.; Bayly, C. I.; Gould, I. R.; Merz, K. M.; Ferguson, D. M.; Spellmeyer, D. C.; Fox, T.; Caldwell, J. W.; Kollman, P. A., A Second Generation Force Field for the Simulation of Proteins, Nucleic Acids, and Organic Molecules. *Journal of the American Chemical Society* **1995,** 117, (19), 5179-5197.

33.   Asensio, J. L.; Martin-Pastor, M.; Jimenez-Barbero, J., The use of CVFF and CFF91 force fields in conformational analysis of carbohydrate molecules. Comparison with AMBER molecular mechanics and dynamics calculations for methyl α-lactoside. *International Journal of Biological Macromolecules* **1995,** 17, (3–4), 137-148.

36

34.   Raffaini, G.; Ganazzoli, F., Sequential adsorption of proteins and the surface modification of biomaterials: A molecular dynamics study. *J Mater Sci: Mater Med* **2007,** 18, (2), 309-316.

35.   Hansen, J.; McDonald, I. R., *Theory of Simple Liquids*. Academic Press Inc: 1986.

36.   Sotomayor, M.; Schulten, K., Single-Molecule Experiments in Vitro and in Silico. *Science* **2007,** 316, (5828), 1144-1148.

37.   Hoover, W. G., Canonical dynamics: Equilibrium phase-space distributions. *Physical Review A* **1985,** 31, (3), 1695-1697.

38.   Nose, S., A unified formulation of the constant temperature molecular dynamics methods. *The Journal of Chemical Physics* **1984,** 81, (1), 511-519.

39.   Parr, R. G. Y., *Density-Functional Theory of Atoms and Molecules*. Oxford University Press: 1994.

40.   Prakash, M.; Subramanian, V., Structure, stability and spectral signatures of monoprotic carborane acid-water clusters (CBWn, where n = 1-6). *Physical Chemistry Chemical Physics* **2011,** 13, (48), 21479-21486.

41.   Boys, S. F.; Bernardi, F., The calculation of small molecular interactions by the differences of separate total energies. Some procedures with reduced errors. *Molecular Physics* **1970,** 19, (4), 553-566.

42.   Frisch, M. J.; Trucks, G. W.; Schlegel, H. B.; Scuseria, G. E.; Robb, M. A.; Cheeseman, J. R.; Scalmani, G.; Barone, V.; Mennucci, B.; Petersson, G. A.; Nakatsuji, H.; Caricato, M.; Li, X.; Hratchian, H. P.; Izmaylov, A. F.; Bloino, J.; Zheng, G.; Sonnenberg, J. L.; Hada, M.; Ehara, M.; Toyota, K.; Fukuda, R.; Hasegawa, J.; Ishida, M.; Nakajima, T.; Honda, Y.; Kitao, O.;

37

Nakai, H.; Vreven, T.; Montgomery, J. J. A.; Peralta, J. E.; Ogliaro, F.; Bearpark, M.; Heyd, J. J.; Brothers, E.; Kudin, K. N.; Staroverov, V. N.; Kobayashi, R.; Normand, J.; Raghavachari, K.; Rendell, A.; Burant, J. C.; Iyengar, S. S.; Tomasi, J.; Cossi, M.; Rega, N.; Millam, J. M.; Klene, M.; Knox, J. E.; Cross, J. B.; Bakken, V.; Adamo, C.; Jaramillo, J.; Gomperts, R.; Stratmann, R. E.; Yazyev, O.; Austin, A. J.; Cammi, R.; Pomelli, C.; Ochterski, J. W.; Martin, R. L.; Morokuma, K.; Zakrzewski, V. G.; Voth, G. A.; Salvador, P.; Dannenberg, J. J.; Dapprich, S.; Daniels, A. D.; Farkas, Ö.; Foresman, J. B.; Ortiz, J. V.; Cioslowski, J.; Fox, D. J., Gaussian~09 Revision A.1. In.

43.   Luzar, A.; Chandler, D., Hydrogen-bond kinetics in liquid water. *Nature* **1996,** 379, (6560), 55-57.

44.   Kumar, R.; Schmidt, J. R.; Skinner, J. L., Hydrogen bonding definitions and dynamics in liquid water. *The Journal of Chemical Physics* **2007,** 126, (20), 204107-12.

45.   Pal, S.; Bandyopadhyay, S., Importance of Protein Conformational Motions and Electrostatic Anchoring Sites on the Dynamics and Hydrogen Bond Properties of Hydration Water. *Langmuir* **2013,** 29, (4), 1162-1173.

46.   Haile, J. M., *Molecular Dynamics Simulation*. John Wiley & Sons, Inc.: New York, 1992.

47.   Ackbarow, T.; Chen, X.; Keten, S.; Buehler, M. J., Hierarchies, Multiple Energy Barriers, and Robustness Govern the Fracture Mechanics of α-Helical and β-Sheet Protein Domains. *Proceedings of the National Academy of Sciences of the United States of America* **2007,** 104, (42), 16410-16415.

48.   Bell, G. I., Models for the specific adhesion of cells to cells. *Science* **1978,** 200, (4342), 618-627.

49.   Lu, H.; Schulten, K., The Key Event in Force-Induced Unfolding of Titin's

Immunoglobulin Domains. *Biophysical Journal* **2000,** 79, (1), 51-65.

50.   Gao, M.; Craig, D.; Lequin, O.; Campbell, I. D.; Vogel, V.; Schulten, K., Structure and

functional significance of mechanically unfolded fibronectin type III1 intermediates.

Proceedings of the National Academy of Sciences **2003,** 100, (25), 14784-14789.

51.   Volkersen, O., Die Nietkraftverteilung in zugbeanspruchten Nietverbindungen mit

konstantin Lenschenquerschnit. *Luftfahrtforschung* **1938,** 15, 41-47.

52.   Beyerlein, I. J.; Landis, C. M., Shear-lag model for failure simulations of unidirectional

fiber composites including matrix stiffness. *Mechanics of Materials* **1999,** 31, (5), 331-350.

53.   Jäger, I.; Fratzl, P., Mineralized Collagen Fibrils: A Mechanical Model with a Staggered

Arrangement of Mineral Particles. *Biophysical Journal* **2000,** 79, (4), 1737-1746.

54.   Nairn, J. A., On the use of shear-lag methods for analysis of stress transfer in

unidirectional composites. *Mechanics of Materials* **1997,** 26, (2), 63-80.

55.   Chen, B.; Wu, P. D.; Gao, H., A characteristic length for stress transfer in the

nanostructure of biological composites. *Composites Science and Technology* **2009,** 69, (7–8),

1160-1164.

56.   Liu, Y.; Xie, B.; Zhang, Z.; Zheng, Q.; Xu, Z., Mechanical properties of graphene papers.

Journal of the Mechanics and Physics of Solids **2012,** 60, (4), 591-605.

57.   Wei, X.; Naraghi, M.; Espinosa, H. D., Optimal Length Scales Emerging from Shear

Load Transfer in Natural Materials: Application to Carbon-Based Nanocomposite Design. *ACS

Nano* **2012,** 6, (3), 2333-44.

39

58.   Sakurada, I.; Kaji, K.; Nakamae, K.; Wadano, S., Experimental Determination of the Elastic Moduli of Polymer Crystals in the Direction Perpendicular to the Chain Axis. *Bulletin of the Institute for Chemical Research* **1966,** 44, (2).

59.   Shahsavari, R.; Buehler, M. J.; Pellenq, R. J. M.; Ulm, F.-J., First-Principles Study of Elastic Constants and Interlayer Interactions of Complex Hydrated Oxides: Case Study of Tobermorite and Jennite. *Journal of the American Ceramic Society* **2009,** 92, (10), 2323-2330.

60.   Argon, A. S.; Demkowicz, M. J., What Can Plasticity of Amorphous Silicon Tell Us about Plasticity of Metallic Glasses? *Metall and Mat Trans A* **2008,** 39, (8), 1762-1778.

61.   Mott, P. H.; Argon, A. S.; Suter, U. W., Atomistic modelling of cavitation of glassy polymers. *Philosophical Magazine A* **1993,** 68, (3), 537-564.

62.   Yu, Y. H.; Lin, C. Y.; Yeh, J. M.; Lin, W. H., Preparation and properties of poly(vinyl alcohol)-clay nanocomposite materials. *Polymer* **2003,** 44, (12), 3553-3560.

1
2
3
4
5
6
7
8
9
10
11
12
13
14
15
16
17
18
19
20
21
22
23
24
25
26
27
28
29
30
31
32
33
34
35
36
37
38
39
40
41
42
43
44
45
46
47
48
49
50
51
52
53
54
55
56
57
58
59
60

TOC Graphic.